THE JOURNAL OF PHYSICAL CHEMISTRY C

Article

pubs.acs.org/JPCC

# Strong Wavelength Dependence of Hyperpolarizability in the Near-Infrared Biological Window for Second-Harmonic Generation by Amphiphilic Porphyrins

Kurt De Mey,*[,†] Javier Perez-Moreno,[†] James E. Reeve,[‡] Ismael Lopez-Duarte,[‡] Igor Boczarow,[‡] Harry L. Anderson,[‡] and Koen Clays[†,§]

[†]Department of Chemistry, University of Leuven, Celestijnenlaan 200D, B-3001 Heverlee, Belgium

[‡]Department of Chemistry, University of Oxford, Chemistry Research Laboratory, Oxford, OX1 3TA, United Kingdom

[§]Department of Physics and Astronomy, Washington State University, Pullman, Washington 99164-2814, United States



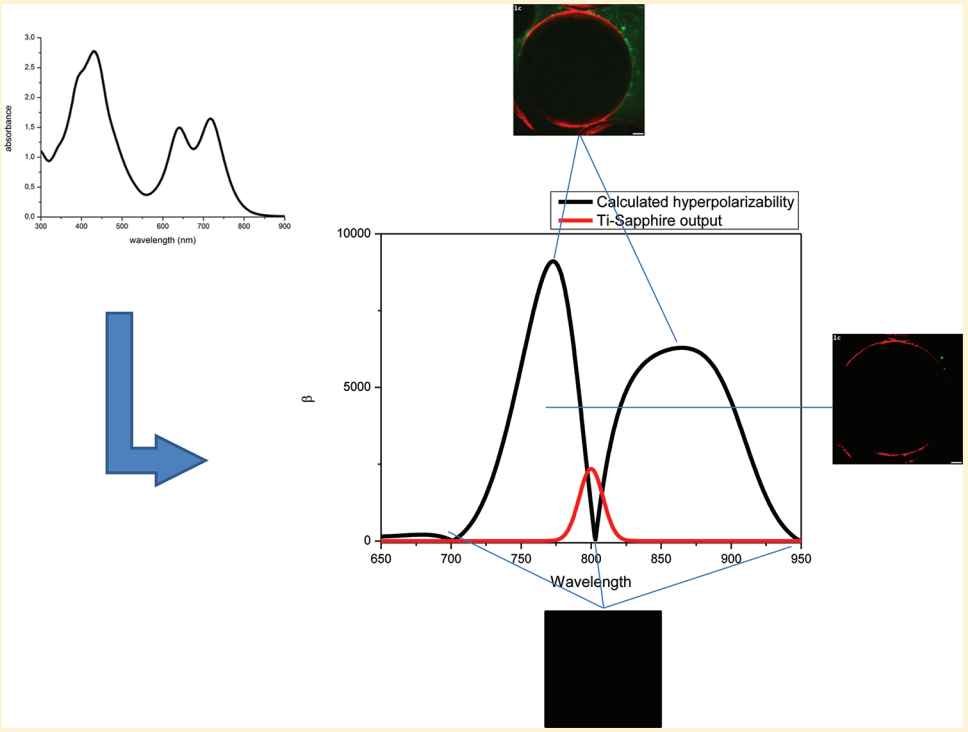


**ABSTRACT:** We have applied the Thomas-Kuhn sum rules to model the wavelength dependence of the second-order nonlinear polarizability of an amphiphilic porphyrin chromophore designed for cellular imaging on the basis of the complete analysis of its linear absorption spectrum. We predict huge oscillations for this first hyperpolarizability in the biological transparency window with the second-order response exhibiting three minima and two maxima in the wavelength range between 700 and 900 nm and a second region of enhanced response between 1200 and 1500 nm. We confirmed the predicted values experimentally demonstrating both the validity of our approach and the need for a wavelength scan to find a maximum in the resonance-enhanced signal for cellular imaging. These results suggest a new approach toward achieving spectroscopic selectivity during second-harmonic generation imaging.

## INTRODUCTION

Second-harmonic imaging microscopy (SHIM) has been established as a nondestructive imaging modality,[1] which is now widely being applied for both basic research and clinical pathology. The second-harmonic generation from certain membrane-bound dyes is highly sensitive to membrane potential. SHIM is already applied as a valuable tool for probing cell physiology, but the small signal amplitude limits

**Received:** March 1, 2012
**Revised:** May 21, 2012
**Published:** May 31, 2012

   dx.doi.org/10.1021/jp302050j | J. Phys. Chem. C 2012, 116, 13781−13787

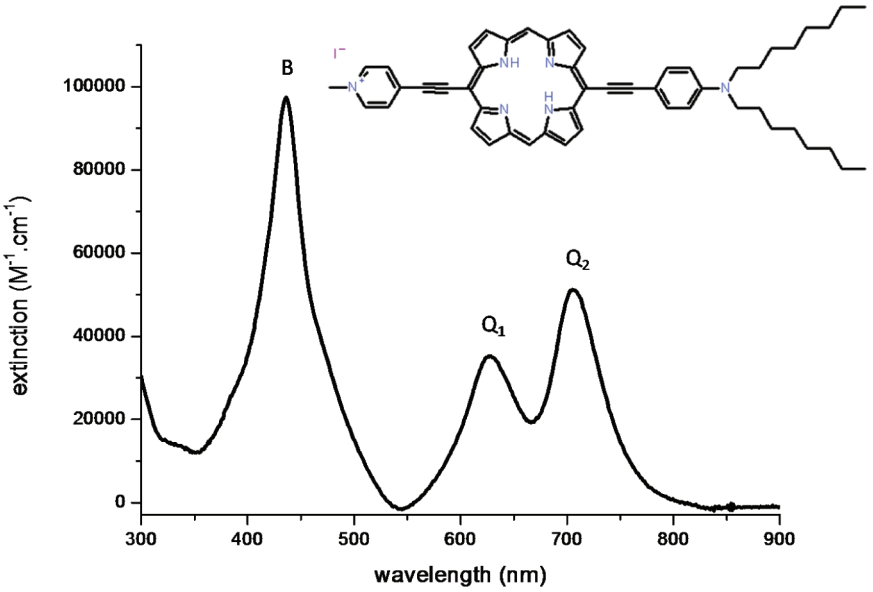


**Figure 1.** Chemical structure and extinction spectrum of chromophore **1** in $CHCl_3$. The two Q-bands are clearly distinguishable ($\lambda_{max}(Q_1)$ = 628 nm, $\lambda_{max}(Q_2)$ = 705 nm) as is the broad Soret or B-band ($\lambda_{max}(B)$ = 436 nm), which will have to be modeled with at least two peaks because of the shoulder around 375 nm.

the number of photons that can be collected during the course of a fast action potential. One of the main challenges in this field is hence the design of more efficient dyes to improve signal-to-noise ratios while still maintaining biocompatibility. SHIM dyes are exogenous chromophores that have a strong two-photon resonance-enhanced nonlinearity in the biological transparency window (700−900 nm) because of an electron donor−acceptor charge-transfer band in the visible region. The early SHIM dyes were one-dimensional conjugated $\pi$-systems,[2] but the current state-of-the-art dyes include multidimensional porphyrin- or carbazole-based chromophores.[3,4] The donor-$\pi$-acceptor porphyrins have strong oscillator strengths along the long molecular axis while also possessing a significant off-diagonal linear and nonlinear polarizability tensor component. Different strategies have been applied to tune the absorption bands to exploit resonance enhancement at different driving frequencies.[5] The transparency window of biological tissue lies between 700 and 900 nm implying that the fundamental wavelength of the incoming probing light should also be in this window. A commercially available titanium$^{3+}$-sapphire laser has a tunable output wavelength exactly over this wavelength range, which makes this one of the most used laser sources for second-harmonic generation imaging.[6] Porphyrins exhibit, in addition to their typical Q bands to the red end of the visible spectrum, a Soret absorption band (or B band) around 400 nm inducing strong resonance enhanced nonlinearities when illuminated with fundamental laser light originating in the biotransparency window. To qualitatively guide research efforts toward enhanced optical nonlinearities, the two-level model of Oudar and Chemla[7] has been traditionally used, where the hyperpolarizability $\beta$ is described in terms of the magnitude of the dipole moments of the ground state ($\mu_{00}$) and a single excited state ($\mu_{11}$), the difference in energy between the ground-state $E_0$ and this excited-state $E_1$, and the interaction between ground and excited state as described in the transition dipole moment $\mu_{01}$

$$\beta \propto (\mu_{11} - \mu_{00}) \frac{\mu_{01}^2}{(E_1 - E_0)^2} \quad (1)$$

This simplified expression for $\beta$ has been used for many years to explain the observed hyperpolarizability dispersion mainly in terms of the resonance enhancement because of the energy difference in the denominator. This transition energy is directly related to the wavelength of maximal linear (one-photon) absorption. For the simplest chromophores, whose light-matter interaction is dominated by a single-charge-transfer transition often in the visible region, the more general sum-over-states (SOS) expression (eq 2) indeed reduces this to a simple two-level model. However, in trying to optimize the hyperpolarizability $\beta$, more complex molecular architectures need to be considered. The electronic interactions of these more complex chromophores can no longer be described by the simple two-level model as they are no longer dependent on only ground and (first) excited states. Interactions between ground and second, third, ... excited states as well as interactions between excited states will play an important role. It has been shown that the generation of a second-order nonlinear optical (NLO) response requires a minimum of three levels,[8] and we will take into account more levels if this proves to be beneficial for the accuracy of our modeling of the linear absorption spectrum. Indeed, the success of our modeling of the nonlinear response is strongly dependent on the quality of the modeling of the linear absorption. We use modeling of the linear absorption in combination with the Thomas-Kuhn sum (TKS) rules to calculate the entire $\beta$-spectrum, and we demonstrate large oscillations in first hyperpolarizability over the spectral window relevant for imaging of biological samples. These large oscillations can cause important differences in the signal-to-noise ratio as a function of actual near-infrared wavelength used. For simple, single charge-transfer molecules, linear spectroscopy has been used to successfully predict the nonlinear dispersion,[9] but the inherent complexity of the chromophore

introduced by the porphyrin ring requires a somewhat different treatment. We have already reported[3] on the apparent anomalous dispersion of the hyperpolarizability of chromophore **1** (Figure 1). We had observed that the hyperpolarizability is increased by a factor of 2 when changing the fundamental wavelength from 800 to 840 nm. We now further investigate the wavelength dependence of the first hyperpolarizability of this chromophore and model its linear and nonlinear optical spectra for comparison with experimentally determined hyperpolarizabilities at more fundamental wavelengths.

## THEORY

**Sum-Over-States.** Our approach is to use the sum-over-states (SOS) expression for the first hyperpolarizability, which depends on the transition energies, the line widths of these transitions, and the transition dipole moments between ground and excited states, which can all be obtained from linear absorption measurement. However, a hyperpolarizability depends also on the transition dipole moments between excited states, which we will calculate using the TKS rules. This approach has already been introduced by Kuzyk[10] and has been worked out for a set of porphyrin chromophores by Hu et al.[11] Since we have observed that this modeling is very sensitive to changes in the line widths, we decided not to use the line width as a fitting parameter but rather to use an averaged experimental line width to give our model more physical robustness. The SOS expression for the diagonal components of the second-order molecular polarizability for the case of frequency doubling as derived by Orr and Ward[12] is given by

$$\beta_{zzz}(-2\omega;\,\omega,\,\omega) = \Sigma'_{m,n}\mu_{0m}\bar{\mu}_{mn}\mu_{n0}\left[\frac{1}{(E_{m0}-i\Gamma_m-2\omega)(E_{n0}-i\Gamma_n-\hbar\omega)} + \frac{1}{(E_{m0}+i\Gamma_m+\hbar\omega)(E_{n0}+i\Gamma_n+2\hbar\omega)} + \frac{1}{(E_{m0}+i\Gamma_m+\hbar\omega)(E_{n0}-i\Gamma_n-\hbar\omega)}\right] \quad (2)$$

where the prime after the sum indicates that the indices $m$, $n$ run only over the excited states and not over the ground state. This expression is defined as a function of the transition dipole moments $\mu_{n0}$, which correspond to the transition dipole moment between the ground state and the $n$th excited state; the energy differences $E_{0n}$, which correspond to the difference in energy between the ground state and the $n$th excited state; and the line widths $\Gamma_n$, which correspond to the line width of the $n$th transition. Also, the bar operator has been introduced such that

$$\bar{\mu}_{mn} = \begin{cases} \mu_{mn} \text{ if } m \neq n \\ \Delta\mu_{n0} \equiv \mu_{nn} - \mu_{00} \text{ if } m = n \end{cases} \quad (3)$$

**Generalized Thomas-Kuhn Sum Rules.** The evaluation of eq 2 requires the evaluation of transition dipole moments of the type $\mu_{mn}$. These do not contribute to the linear response and, hence, cannot be derived from the linear absorption spectrum and will have to be calculated or measured independently. Therefore, we need to find a mechanism that allows us to calculate the transition dipole moments $\mu_{mn}$ as a function of the transition dipole moments $\mu_{0n}$. One possible approach would be to use computational chemistry methods to calculate the wave function from the molecular structure and then to evaluate the transition dipole moments, a task that is far from trivial. Instead, we use the generalized TKS rules to derive relationships between the transition dipole moments following the approach introduced by Kuzyk for the first time in the calculation of the fundamental limits of the molecular susceptibilities.[13]

$$\sum_n (2E_n - E_k - E_l)\mu_{kn}\mu_{nl} = \frac{e^2\hbar^2 N}{m}\delta_{kl} \quad (4)$$

where $N$ denotes the number of electrons of the system and $\delta_{kl}$ is the Kronecker delta. The evaluation of the transition dipole moments is possible by using the off-diagonal sum rules, which are obtained by evaluating eq 4 with $k \neq l$. The number of equations to be solved can be calculated with binomial coefficients, $\binom{n}{k}$. The number of excited states we take into account plus the ground state gives us $n$, and since by assumption the transition dipole moments are real, $\mu_{ij}$ must be equal to $\mu_{ji}$, and thus $k = 2$.

## RESULTS

**Modeling of the Extinction spectrum.** The linear optical properties were characterized with a Perkin-Elmer UV-2001 spectrometer. The UV−vis spectra were converted to molar extinction, $\varepsilon$ (in units of $M^{-1}$ $cm^{-1}$) using the Lambert−Beer law. The molar extinction spectrum of chromophore **1** as a function of photon wavelength, $\lambda$, is shown in Figure 1. The corresponding extinction spectrum as a function of photon energy in eV is shown in Figure 2 (black circles). The linear absorption spectra exhibits the typical Q-bands that are associated with the porphyrin structure (with $D_{4h}$ symmetry). These types of bands arise from the transitions to orbitally degenerate excited states within the porphyrin ring and are enhanced because of the incorporation of the ring into a donor−acceptor conjugated structure.[14,15] The addition of donor and acceptor groups along the extended conjugated path results also in the enhancement (and red shift) of the B-band, which results from orbitally degenerate transitions between ground and first exited states. Since the B-band arises from the coupling of multiple charge transfer oscillators, the spectral envelope is expected to be broader than for Q-bands because of the overlapping of more close-lying transitions. This is indeed the case for chromophore **1**. The spectrum shows a total of three broad absorption bands: a B-band ($\lambda_{max}^{(1)}$ = 436 nm) and two Q-bands ($\lambda_{max}^{(2)}$ = 628 nm, $\lambda_{max}^{(3)}$ = 705 nm). However, a minimum of four peaks is necessary to model the extinction spectrum (Figure 2).

It is important to realize that to get reliable results from the sum rules, we must be sure that the variables we use to calculate them are reliable. Therefore, we must check that the information we obtain out of the linear extinction is physically correct. We must model the peaks sufficiently accurately to reproduce the experimental extinction profile. For this reason,


dx.doi.org/10.1021/jp302050j | J. Phys. Chem. C 2012, 116, 13781−13787

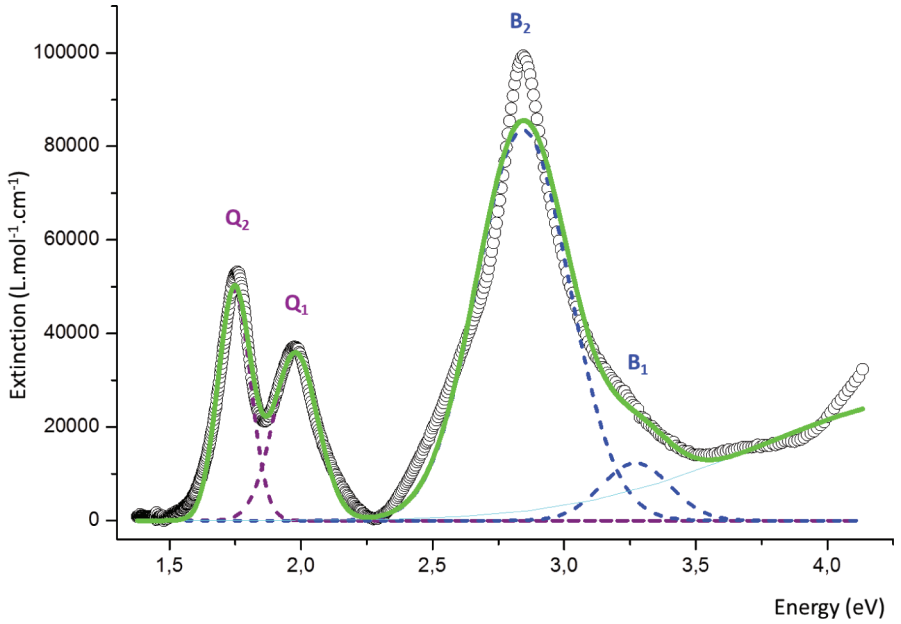


**Figure 2.** Extinction spectrum of chromophore **1** (derived from the spectrum in Figure 1). The spectrum is modeled with five Gaussian peaks. The Q-bands are very straightforward, whereas the B-band needs a minimum of two peaks to be resolved. The broad high energy contribution to the spectrum is fitted with one Gaussian broad band.

although our computational limit lies at four excited states, we must model the extinction spectrum with an additional fifth and very broad feature to account for the slowly rising tail at the high-energy end. This tail, however, is not taken into account in the modeling of the hyperpolarizability because we assume that the behavior of the first hyperpolarizability is dominated by the contributions of the first four excited states: their contributions are resonantly enhanced for the range of fundamental wavelengths used to characterize the first hyperpolarizability. The extinction spectrum is fitted with Gaussian peaks because the dominating broadening effect in solution gives rise to absorption bands with a mainly Gaussian profile.

The energy difference between the $i$th excited state and the ground state, $E_{i0}$ (in eV), is now easily obtained from the values of the wavelength of maximum absorption for each peak (in nm)

$$E_{i0} = \frac{1240}{\lambda_{\max}^{(i)}} \tag{5}$$

Also, when the peak in the molar extinction spectrum can be distinguished from the other peaks, the area under the peak can be related to the corresponding (dressed) oscillator strength[16−18]

$$|\mu_{i0}^{*}|^2 = \left(\frac{9.13 \times 10^{-3}}{E_{i0}}\right) \int_0^{\infty} \varepsilon^{(i)}(E)\mathrm{d}E \tag{6}$$

where $\varepsilon^{(i)}$ is expressed in units of $M^{-1}$ $cm^{-1}$ and $|\mu_{i0}^{*}|$ is in Debye.

The line widths are obtained directly from the fits to the extinction peaks and are defined as the half width at half-maximum (HWHM) of the $i$th transition. For our modeling, we use the average of the line widths we have thus obtained. The experimental parameters obtained are listed in Table 1.

**Table 1. Parameters Describing the Linear (One-Photon) Absorption of Chromophore 1**[a]

| $i$ | $E_{i0}$ (eV) | $\lambda_{\max}$ (nm)[b] | $\lambda_{\max}$ (nm)[c] | $\int_0^{\infty}\varepsilon^{(i)}(E)\,\mathrm{d}E$ | $\lvert\mu_{0i}\rvert$ (D) | $\Gamma_i$ (eV) |
|---|---|---|---|---|---|---|
| 1 | 1.75 | 709 | 705 | 7651 | 6.324 | 0.0727 |
| 2 | 1.98 | 626 | 628 | 7603 | 5.922 | 0.0998 |
| 3 | 2.84 | 437 | 436 | 37 326 | 10.948 | 0.2094 |
| 4 | 3.28 | 378 | ca. 375 | 4166 | 3.407 | 0.1445 |
| *5*[d] | *4.47* | *277* | / | *48 429* | *9.947* | *0.7909* |

[a]The linear behavior was modeled with four significant peaks for the four dominant transitions. [b]The wavelength of maximum absorbance is directly calculated out of the transition energy of the modeled peak. [c]The wavelength of maximum absorbance is determined out of the experimental spectrum. [d]The fifth peak is considered to contain all other transitions and is therefore modeled with a Gaussian broad band, and its data are in italics because they are not taken into account for the modeling.

**Experimental Hyperpolarizability Measurements.** All experimental hyperpolarizabilities of chromophore **1** were determined by hyper-Rayleigh scattering[19,20] in $CHCl_3$ at different tunable setups. Measurements at fundamental infrared wavelengths of 1240, 1300, 1320, 1340, and 1500 nm were carried out on a tunable femtosecond Hyper-Rayleigh Scattering (HRS) setup. This setup uses a diode laser to pump a titanium-sapphire laser (Spectra-Physics, model Tsunami) and an optical parametric oscillator (OPO) (Spectra-Physics OPAL) tunable in the infrared region. Measurements at fundamental near-infrared wavelengths of 800 and 840 nm were carried out at a simplified version of this setup, which was previously described.[21] All experimental hyperpolarizabilities are reported in Table 2. To discriminate between the immediate nonlinear scattering and the time-delayed multiphoton fluorescence, we use high-frequency demodulation technique.[21−23] The earlier reported hyperpolarizability[3] at a fundamental


dx.doi.org/10.1021/jp302050j | J. Phys. Chem. C 2012, 116, 13781−13787

**Table 2. Experimental Hyperpolarizabilities**

| $\lambda$ (nm) | $\hbar\omega$ (eV) | $\beta_{zzz}$( $\times 10^{-30}$ esu) | $\delta\beta_{zzz}$( $\times 10^{-30}$ esu) |
|---|---|---|---|
| 800 | 1.55 | 2500 | 300 |
| 840 | 1.48 | 6500 | 500 |
| 1240 | 1.00 | 500 | 100 |
| 1300 | 0.95 | 800 | 100 |
| 1320 | 0.94 | 1300 | 100 |
| 1340 | 0.93 | 1700 | 100 |
| 1500 | 0.83 | <50[a] | / |

[a]The value at 1500 nm was too small to measure, so an upper limit of $50 \times 10^{-30}$ esu is given.

wavelength of 1064 nm was obtained on a nanosecond Nd:YAG laser system, such that the high-frequency demodulation technique cannot be applied, and it is thus impossible to exclude any fluorescence contribution to this signal. Since we cannot rule out fluorescence for this value, we did not take it further into account in this analysis.

We notice that, in principle, because the first hyperpolarizabilities are complex quantities, one should be careful when extrapolating the diagonal component of the first hyperpolarizability $\beta_{zzz}$ from the experimentally determined orientational averaged hyperpolarizability squared $\langle\beta^2_{\mathrm{HRS}}\rangle$.[24] For polar molecules with $C_{\infty v}$ symmetry where the diagonal component $\beta_{zzz}$ is much larger than $\beta_{zxx}$, such as the molecule considered in our study, a simple relationship is derived assuming Kleinman symmetry

$$\langle\beta^2_{\mathrm{HRS}}\rangle = \frac{6}{35}\beta^2_{zzz} \tag{7}$$

Although we are aware that Kleinman symmetry is only valid away from resonances, for consistency, we have taken the values obtained through hyper-Rayleigh scattering characterization to provide for the real part of $\beta_{zzz}$ through eq 7. While other options are possible, our calculations show that the approximation is valid at the wavelengths of measurement, where the real part of $\beta_{zzz}$ dominates over the imaginary part, and hence, eq 7 holds.

**Hyperpolarizability Spectrum.** Our objective is to apply the SOS expression for the first hyperpolarizability (eq 2) using only the results from the linear absorption characterization. With the TKS rules (eq 4), we now have a tool to provide the missing variables for the hyperpolarizability expression. We use the off-diagonal sum rules to obtain the values of $\mu_{mn}$ as a function of the values of $\mu_{n0}$ (which are obtained from the linear extinction). In our case, we model with four peaks, and thus, we must truncate the sum rules at four excited states, which gives us $\binom{5}{2} = 10$ independent nonlinear equations to solve

$$\begin{cases}
(E_0 - E_1)\mu_{00}\mu_{01} + (E_1 - E_0)\mu_{01}\mu_{11} + (2E_2 - E_0 - E_1)\mu_{02}\mu_{21} \\
+ (2E_3 - E_0 - E_1)\mu_{03}\mu_{31} + (2E_4 - E_0 - E_1)\mu_{04}\mu_{41} = 0 \\
(E_0 - E_2)\mu_{00}\mu_{02} + (2E_1 - E_0 - E_2)\mu_{01}\mu_{12} + (E_2 - E_0)\mu_{02}\mu_{22} \\
+ (2E_3 - E_0 - E_2)\mu_{03}\mu_{32} + (2E_4 - E_0 - E_2)\mu_{04}\mu_{42} = 0 \\
(E_0 - E_3)\mu_{00}\mu_{03} + (2E_1 - E_0 - E_3)\mu_{01}\mu_{13} + (2E_2 - E_0 - E_3)\mu_{02}\mu_{23} \\
+(E_3 - E_0)\mu_{03}\mu_{33} + (2E_4 - E_0 - E_3)\mu_{04}\mu_{43} = 0 \\
(E_0 - E_4)\mu_{00}\mu_{04} + (2E_1 - E_0 - E_4)\mu_{01}\mu_{14} + (2E_2 - E_0 - E_4)\mu_{02}\mu_{24} \\
+(2E_3 - E_0 - E_4)\mu_{03}\mu_{34} + (E_4 - E_0)\mu_{04}\mu_{44} = 0 \\
(2E_0 - E_1 - E_2)\mu_{01}\mu_{02} + (E_1 - E_2)\mu_{11}\mu_{12} + (E_2 - E_1)\mu_{12}\mu_{22} \\
+ (2E_3 - E_1 - E_2)\mu_{13}\mu_{32} + (2E_4 - E_1 - E_2)\mu_{14}\mu_{42} = 0 \\
(2E_0 - E_1 - E_3)\mu_{01}\mu_{03} + (E_1 - E_3)\mu_{11}\mu_{13} + (2E_2 - E_1 - E_3)\mu_{12}\mu_{23} \\
+(E_3 - E_1)\mu_{13}\mu_{33} + (2E_4 - E_1 - E_3)\mu_{14}\mu_{43} = 0 \\
(2E_0 - E_1 - E_4)\mu_{01}\mu_{04} + (E_1 - E_4)\mu_{11}\mu_{14} + (2E_2 - E_1 - E_4)\mu_{12}\mu_{24} \\
+(2E_3 - E_1 - E_4)\mu_{13}\mu_{34} + (E_4 - E_1)\mu_{14}\mu_{44} = 0 \\
(2E_0 - E_2 - E_3)\mu_{02}\mu_{03} + (2E_1 - E_2 - E_3)\mu_{21}\mu_{13} + (E_2 - E_3)\mu_{22}\mu_{23} \\
+(E_3 - E_2)\mu_{23}\mu_{33} + (2E_4 - E_2 - E_3)\mu_{24}\mu_{43} = 0 \\
(2E_0 - E_2 - E_4)\mu_{02}\mu_{04} + (2E_1 - E_2 - E_4)\mu_{21}\mu_{14} + (E_2 - E_4)\mu_{22}\mu_{24} \\
+(2E_3 - E_2 - E_4)\mu_{23}\mu_{34} + (E_4 - E_2)\mu_{24}\mu_{44} = 0 \\
(2E_0 - E_3 - E_4)\mu_{03}\mu_{04} + (2E_1 - E_3 - E_4)\mu_{31}\mu_{14} + (2E_2 - E_3 - E_4)\mu_{32}\mu_{24} \\
+ (E_3 - E_4)\mu_{33}\mu_{34} + (E_4 - E_3)\mu_{34}\mu_{44} = 0
\end{cases}$$


dx.doi.org/10.1021/jp302050j | J. Phys. Chem. C 2012, 116, 13781−13787

These equations give rise to 64 sets of mathematically correct solutions, real and imaginary, of which all the real sets should be considered and checked against the experimental hyperpolarizabilities. Only one of these sets of mathematical solutions provides a hyperpolarizability spectrum that agrees with the experimental data and is thus the physically correct one. The results of the TKS rules are presented in Table 3.

**Table 3. Transition Dipole Moments $\mu_{nm}$ (Debye) between Excited States Are Calculated through the Mathematica Software**

| $\mu_{ij}$ | 0 | 1 | 2 | 3 | 4 |
|---|---|---|---|---|---|
| 0 | $\mu_{00}$ | $\mu_{01}$ | $\mu_{02}$ | $\mu_{03}$ | $\mu_{04}$ |
| 1 | $\mu_{10}$ | −24.66 | −5.204 | −3.354 | 29.63 |
| 2 | $\mu_{20}$ | $\mu_{21}$ | −9.881 | −35.98 | 1.769 |
| 3 | $\mu_{30}$ | $\mu31$ | $\mu_{32}$ | −0.525 | 7.548 |
| 4 | $\mu_{40}$ | $\mu_{41}$ | $\mu_{42}$ | $\mu_{34}$ | −22.12 |

The solution set with opposite sign is equally correct because we always measure $\beta^2$, and thus the sign is undetermined. To check for the correct solution, we thus consider the absolute value of the hyperpolarizability spectrum.

In the Beratan model,[11] the line widths of all the peaks are set equal to the same effective line width value, Γ, which is treated as a fitting parameter, while the values of the transition energies are allowed to be lower than the measured values through the peaks on the linear absorption by a factor $S_v \leq 1$. Typical values for $S_v$ are between 0.90 and 0.99. This energy shift (lowering the measured energy from $E_{n0}$ to $S_v \cdot E_{n0}$) is based on the fact that the experimentally measured transition bands might be peaked at energies above the electronic origin because of the shape of the Franck−Condon envelope. In our approach, we still use $S_v$ as a fitting parameter, but we use the average experimental line width obtained from our modeling of the linear spectrum. In this way, because our modeling is dependent on the line width, we achieve added robustness. We assume that the behavior of the first hyperpolarizability is dominated by the contributions of the first four excited states since their contributions are resonantly enhanced for the range of fundamental wavelengths used to characterize the first hyperpolarizability. Therefore, we truncate the sum rules, including up to the fourth excited state, because for the sake of simplicity, we only solve the 10 equations corresponding to 4 excited states.

As can be seen in Figure 3, the subtle electronic interplay between the excited states comprising the B-band in the absorption spectrum (around 400 nm) gives rise to strong oscillations in the hyperpolarizability value when illuminated with fundamental light around 800 nm. In fact, with oscillations at a maximum of 775, 860, and 1400 nm, the hyperpolarizability exhibits two maxima and three minima in barely 85 nm. While the spectral content for a femtosecond pulse is broad (full width at half-maximum (fwhm) 20 nm), it is still narrow with respect to the oscillatory features as shown in the inset of Figure 3. Also, the Q-band envelope gives rise to the smaller oscillations when illuminated with ∼1300 nm. Our model predicts a minimum (zero crossing when considering absolute value) at a fundamental wavelength of ∼1530 nm, which was corroborated by the measurement at 1500 nm which gave no measurable hyperpolarizability.

**Conclusions and Perspectives.** A strong oscillatory wavelength dependence for the second-order nonlinear polarizability (first hyperpolarizability $\beta$) of a donor−acceptor substituted porphyrin chromophore has been modeled on the basis of its linear absorption and the Thomas-Kuhn sum rules. Within the relative narrow wavelength range of the optical transparency window (700−900 nm), extreme variation in the first hyperpolarizability is modeled and experimentally verified. The validity of the approach is corroborated by experimental hyperpolarizabilities confirming the modeling in the near-infrared beyond this transparency window (1240−1500 nm). The important implication of this result is that the exact fundamental wavelength for cellular imaging using this membrane-specific probe has a primary effect on the signal-to-noise ratio. A simple wavelength scan over the available tuning range of the laser of choice, that is, a Ti-sapphire laser, can suffice to maximize the signal. An intriguing perspective is offered when considering that the transition energies, determining the detailed spectral features of the wavelength

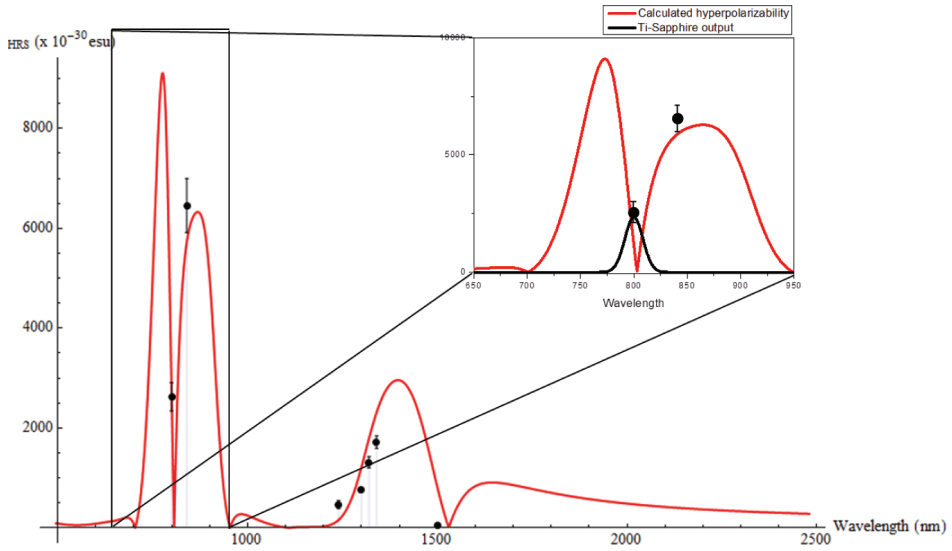


**Figure 3.** Calculated dispersion of the first hyperpolarizability of chromophore **1** (line) and experimental values (points) in the wavelength domain. (Inset) Calculated hyperpolarizability (red) between 650 and 950 nm with the typical Gaussian spectral content of a femtosecond laser pulse (black) from a Ti-sapphire laser.


dx.doi.org/10.1021/jp302050j | J. Phys. Chem. C 2012, 116, 13781−13787

dependence, are a function of the substitution on the porphyrin ring. By using differently substituted porphyrins, the different absorption spectra will give rise to different spectral features for the nonlinear polarizability. Given the sharpness of these features, the possibility emerges to spectrally select one imaging probe by setting the fundamental wavelength to the zero response of the other probe providing selective imaging of two (or more) probes.

## AUTHOR INFORMATION

### Corresponding Author

*E-mail: kurt.demey@fys.kuleuven.be. Phone: +3216327523.

### Notes

The authors declare no competing financial interest.

## ACKNOWLEDGMENTS

The authors would like to thank EPSRC (EP/H018565/1) and FWO-V (G.0312.08) for funding and the European Commission for the Marie Curie Intra-European Fellowship for I. Lopez-Duarte. J.P.M. acknowledges the KULeuven IDO project 3E090505.

## REFERENCES

(1) Campagnola, P. J.; Moew, L. M. Second-harmonic imaging microscopy for visualizing biomolecular arrays in cells, tissues and organisms. *Nat. Biotechnol.* **2003**, *21*, 1356−1360.

(2) Reeve, J. E.; Anderson, H. L.; Clays, K. Dyes for biological second harmonic generation imaging. *Phys. Chem. Chem. Phys.* **2009**, *12* (41), 13484−98.

(3) Reeve, J. E.; Collins, H. A.; De Mey, K.; Kohl, M. M.; Thorley, K. J.; Paulsen, O.; Clays, K.; Anderson, H. L. Amphiphilic porphyrins for second harmonic generation imaging. *J. Am. Chem. Soc.* **2009**, *131* (8), 2758−2759.

(4) De Meulenare, E.; Chen, W.-Q.; Van Cleuvenbergen, S.; Zheng, M.-L.; Psilodimitrakopoulos, S.; Paesen, R.; Taymans, J.-M.; Ameloot, M.; Vanderleyden, J.; Loza-Alvarez, P.; Duan, X.-M.; Clays, K. Molecular engineering of chromophore for combined second-harmonic and two-photon fluorescence in cellular imaging. *Chem. Sci.* **2012**, *3* (4), 984−995.

(5) Therien, M. J. How to improve your image. *Nature* **2009**, *458* (7239), 716.

(6) Yasui, T. Ex vivo and in vivo second-harmonic-generation imaging of dermal collagen fiber in skin: comparison of imaging characteristics between mode-locked Cr:forsterite and Ti:sapphire lasers. *Appl. Opt.* **2009**, *48* (10), 88−96.

(7) Oudar, J. L.; Chemla, D. S. Hyperpolarizabilities of the nitroanilines and their relations to the excited state dipole moment. *J. Chem. Phys.* **1977**, *66* (6), 2664−2668.

(8) Perez-Moreno, J.; Clays, K.; Kuzyk, M. Why do we need three levels to understand the molecular optical response? *SPIE Proc.* **2011**, *8113*, No. , DOI: 10.1117/12.893477.

(9) Perez-Moreno, J.; Hung, S.-T.; Kuzyk, M.; Zhou, J.; Ramini, S. K.; Clays, K. Experimental verification of a self-consistent theory of the first-, second-, and third-order (non)linear response. *Phys. Rev. A* **2011**, *84*, 033837.

(10) Kuzyk, M. G. Fundamental Limits on Nonlinear Susceptibilities. *Opt. Photonics News* **2003**, *14* (12), 26.

(11) Hu, X.; Xiao, D.; Keinan, S.; Asselberghs, I.; Therien, M. J.; Clays, K.; Yang, W. T.; Beratan, D. N. Predicting the frequency dispersion of electronic hyperpolarizabilities on the basis of absorption data and Thomas-Kuhn sum rules. *J. Phys. Chem. C* **2010**, *114*, 2349−2359.

(12) Orr, B. J.; Ward, J. F. Perturbation Theory of the Non-Linear Optical Polarization of an Isolated System. *Mol. Phys.* **1971**, *20* (3), 513−526.

(13) Kuzyk, M. G. Physical Limits on Electronic Nonlinear Molecular Susceptibilities. *Phys. Rev. Lett.* **2000**, *85*, 1218−1221.

(14) Karki, L.; Vance, F. W.; Hupp, J. T.; LeCours, S. M.; Therien, M. J. Electronic stark effect studies of a porphyrin-based push-pull chromophore displaying a large first hyperpolarizability: state-specific contributions to *β*. *J. Am. Chem. Soc.* **1998**, *120* (11), 2606−2611.

(15) Uyeda, H. T.; Zhao, Y.; Wostyn, K.; Asselberghs, I.; Clays, K.; Persoons, A.; Therien, M. J. Unusual frequency dispersion effects of the nonlinear optical response in highly conjugated (polypyridyl)-metal(porphinato)zinc(ii) chromophores. *J. Am. Chem. Soc.* **2002**, *124* (46), 13806−13813.

(16) Tripathy, K.; Pérez Moreno, J.; Kuzyk, M. G.; Coe, B. J.; Clays, K.; Kelley, A. M. Why hyperpolarizabilities Fall Short of the Fundamental Quantum Limits. *J. Chem. Phys.* **2004**, *121* (16), 7932−7945.

(17) Tripathy, K.; Pérez Moreno, J.; Kuzyk, M. G.; Coe, B. J.; Clays, K.; Kelley, A. M. Erratum: Why Hyperpolarizabilities Fall Short of the Fundamental Quantum Limits. *J. Chem. Phys.* **2006**, *125*, 079905.

(18) Pérez Moreno, J. Theoretical and experimental characterization of the first hyperpolarizability. PhD thesis, WA State University & K.U. Leuven, 2007.

(19) Clays, K.; Persoons, A. Hyper-Rayleigh Scattering in Solution. *Phys. Rev. Lett.* **1991**, *66* (23), 2980−2983.

(20) Clays, K.; Persoons, A. Hyper-Rayleigh Scattering in Solution. *Rev. Sci. Instrum.* **1992**, *63* (6), 3285−3289.

(21) Olbrechts, G.; Strobbe, R.; Clays, K.; Persoons, A. High-frequency demodulation of multi-photon fluorescence in hyper-Rayleigh scattering. *Rev. Sci. Instrum.* **1998**, *69*, 2233.

(22) Olbrechts, G.; Wostyn, K.; Clays, K.; Persoons, A. High-frequency demodulation of multiphoton fluorescence in long-wavelength hyper-Rayleigh scattering. *Opt. Lett.* **1999**, *24* (6), 403−405.

(23) Clays, K.; K. Wostyn, B. K.; Persoons, A. Hyper-Rayleigh scattering in the Fourier domain for higher precision: Correcting for multi-photon fluorescence with demodulation and phase data. *Rev. Sci. Instrum.* **2001**, *72* (8), 3215−3220.

(24) Verbiest, T.; Clays, K.; Rodriguez, V. *Second-order nonlinear optical characterization techniques*; CRC Press: Boca Raton, FL, 2009.